DNS of turbulent low Mach channel flow under asymmetric high temperature gradient: Effect of thermal boundary condition on turbulence statistics

J.M. Avellaneda, F. Bataille, Adrien Toutant

DNS of turbulent low Mach channel flow under asymmetric high temperature gradient: effect of thermal boundary condition on turbulence statistics

J.M. Avellaneda[a,*], F. Bataille[a], A. Toutant[a]

[a] *PROMES-CNRS, UPR 8521, University of Perpignan Via Domitia, Perpignan, France*

Abstract

Direct Numerical Simulations have been performed for a fully-developed low Mach turbulent flow of an ideal gas with thermo-dependent viscosity and thermal conductivity in a flat channel at mean friction Reynolds number $Re_\tau = 180$ submitted to asymmetric heating with a wall temperature ratio $T_2/T_1 = 2$. Mean and turbulent statistics of the flow have been studied and compared for two different thermal boundary conditions: fixed temperatures on the one hand and fixed heat flux densities on the other hand. The influence of the boundary condition type is studied. Temperature variance is particularly impacted by this choice and exhibits asymmetric profiles with different behavior depending on the boundary condition.

Keywords: Turbulence, Direct Numerical Simulation, Channel flow, Asymmetric heating, Low Mach

1. Introduction

Since the seminal works of Orzag [1], Kim [2] and Moser [3], Direct Numerical Simulations (DNS) have proved to be a reference tool to study wall-bounded turbulent flows and have lead to numerous publications. Vreman [4] made a comparison of several of the resulting databases at $Re_\tau = 180$, a popular turbulent Reynolds number, and assessed their accuracy and reproducibility. Among the research works presenting a thermal analysis and in particular the profiles of temperature fluctuations, some are dealing with incompressible flows and assume the temperature to be a passive scalar [5], which can be an appropriate approximation when temperature gradients are small. However, in a large number of industrial applications and thermal exchangers, the gradient of temperature can be high and temperature dependent material properties must be considered. This is the case, for example, in solar receivers [6] [7] [8] [9] [10], a key device in concentrated solar power plants which is worth optimizing [11]. The coupling between turbulence and significant thermal fluxes is studied thoroughly in the case of high-speed compressible flows [12] [13] [14] [15] [16] [17] but more rarely when the flow is subsonic and the fluid properties vary with the temperature [18] [19].

Moreover, the type of thermal boundary condition at the walls has an impact on the turbulent flow and on temperature fluctuations in particular. Many studies impose constant and uniform wall temperatures. For example, Dhamarathne [20] performed DNS of an incompressible channel flow with temperature treated as a passive scalar at $Re_\tau = 395$ and $Pr = 0.71$ while setting dimensionless wall temperatures to -1 and 1 respectively. He shows that the temperature fluctuation standard deviation vanishes at the walls, reaches a local maximum near the wall and then decreases to a local minimum before growing again up to the central zone of the channel. Staying in the case of incompressible flow and of passive scalar temperature, other research works deal with constant and uniform heat flux density at the walls. Different geometries have been addressed, some by Large Eddy Simulations, among which flows in tubes [21] [22], in annuli [23] [24], in rotating cylinders [25] [26] and in flat plate channels [27] [28] [29].

A part of these studies set a strong constraint on temperature fluctuations by forcing them to be zero at the walls (e.g.: [22], [25]), while other leave temperature fluctuation free (e.g. [23], [24]).

Estimating temperature variance at the walls is necessary when thermal fatigue and long-term aging of materials are at stake. Several authors compare the influ-

*Corresponding author
Email address: jean-marc.avellaneda@promes.cnrs.fr (J.M. Avellaneda)

ence of thermal boundary condition type on the flow statistics, by analyzing fluid-solid conjugation. Flageul et al. [30] compared several thermal boundary condition types (Dirichlet isothermal, Neumann isoflux, Robin and 3D fluid-solid conjugate heat transfer) and confirmed the strong impact of the boundary condition on turbulent thermal correlation coefficients and on the variance of temperature. Tiselj et al. [31] [32] [33] also compared fluid-solid conjugation and idealized thermal boundary conditions and showed that wall temperature fluctuations depend on the fluid versus wall effusivity ratio (at the limit, when this ratio tends towards zero, the fluctuations of temperature are zero at the wall).

Nevertheless, these studies focus on incompressible and passive scalar flows. Recently, Bellec et al. [34] performed a comparison between fixed temperature vs. imposed heat flux boundary condition based upon Large Eddy Simulations for a subsonic turbulent flow in an open channel and a fluid with variable properties. To the best of our knowledge, there is no Direct Numerical Simulation equivalent comparison for a fully-developed turbulent low Mach channel flow in the presence of high temperature gradient from non-symmetric heating with thermo-dependent fluid properties. This is the scope of the present work. It can be applied, for example, to the solar receivers of concentrated solar power plants where low Mach flow turbulent temperature fluctuations contribute to the thermal stress of stretched materials.

2. Numerical method

2.1. Governing equations

We focus on low Mach number flows for which the characteristic fluid velocity is small against the speed of sound. In a (strictly) incompressible flow, the density of each fluid particle stays unchanged (the material derivative $D\rho/Dt$ is zero, which implies that the velocity vector is divergence free). A particular situation where the flow is incompressible is when the fluid has a uniform and constant density. In a large number of flows of practical interest, the density variations of a fluid particle are negligibly small and the simplified governing equations of the incompressible flow can be applied without losing excessive precision, one necessary condition being a small Mach number: $Ma << 1$ [35]. This is the case in aerodynamics when the $Ma < 1/3$ criteria is used [36]. Nevertheless, even if the Mach number is small, significant density variations can come from high temperature gradients and the incompressible flow model is no longer suitable. To address this specific situation, a low Mach approximation can be defined by filtering acoustic waves [37] while keeping density variations due to the temperature. This low Mach approximation allows better efficiency in numerical solving the governing equations of this kind of flow in comparison with compressible models because the Courant-Friedrichs-Lewy (CFL) stability conditions on the time step are less severe [18]. In this paper we consider situations where $Ma \approx 10^{-2}$ and a hot to cold wall temperature ratio $T_2/T_1 \approx 2$ over a short distance, leading to corresponding high density variation as the study fluid is an ideal gas: this makes the low-Mach approximation a reasonable approach. In the present study simulations, the density varies with the temperature and buoyancy forces are necessarily present, although their effect is not significant. The relative importance of inertial and buoyancy effects has to be assessed in order to decide whether buoyancy may be neglected or not. The Richardson number $Ri = Gr/Re^2$, where Gr is the Grashof number reflects this relative importance [38]. When $Ri < 0.1$ the flow is generally considered as being dominated by forced convection [39] [40]. For $Ri > 10$, natural convection is the main phenomena and the case where $0.1 \leq Ri \leq 10$ corresponds to mixed convection situations, where natural and forced convection have to be taken in consideration together. For the simulations presented in our manuscript, the Richardson number is small ($Ri \approx 0.01$) and the forced convection flow regime can be considered [41] [18]. Moreover, the fluid flows between two horizontal plates (fig. 1), the channel height is small and the hot plate is the upper one (which corresponds to a beam-down solar receiver, for example). For all these reasons, gravity effects and buoyancy force terms are neglected in the set of governing equations. We assume there is no heat source in the volume and no radiative thermal transfer inside the channel. In the case of an ideal gas, this set of hypothesis leads to a simplified form of the Navier-Stokes equations which now read [37]:

$$\frac{\partial \rho}{\partial t} + \frac{\partial (\rho U_j)}{\partial x_j} = 0 \tag{1}$$

$$\begin{aligned} \frac{\partial (\rho U_i)}{\partial t} + \frac{\partial (\rho U_i U_j)}{\partial x_j} = -\frac{\partial P_{dyn}}{\partial x_i} \\ + \frac{\partial}{\partial x_j}\left[\mu\left(\frac{\partial U_i}{\partial x_j} + \frac{\partial U_j}{\partial x_i}\right)\right] - \frac{2}{3}\frac{\partial}{\partial x_j}\left(\mu \frac{\partial U_k}{\partial x_k}\right) \end{aligned} \tag{2}$$

$$\rho C_p\left(\frac{\partial T}{\partial t} + U_j \frac{\partial T}{\partial x_j}\right) = \frac{\partial P_{th}}{\partial t} + \frac{\partial}{\partial x_j}\left(k \frac{\partial T}{\partial x_j}\right) \tag{3}$$

$$\frac{\partial P_{th}}{\partial x_i} = 0 \tag{4}$$

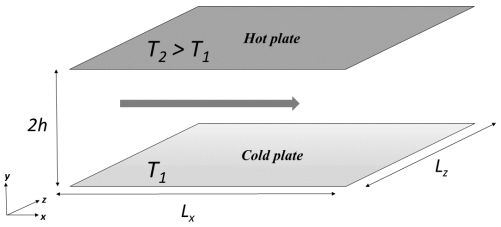

Figure 1:

In this system of equations the subscripts i and j obey the summation convention and ρ is the density of the fluid, U_i are the components of its velocity, μ is its dynamic viscosity, $C_p = 1005\ J.kg^{-1}K^{-1}$ is its heat capacity, k is its thermal conductivity and T is its temperature. x_i are the Cartesian coordinates and t is the time. Pressure is composed of two terms: $P = P_{dyn} + P_{th}$ where P_{dyn} accounts for the variations of pressure due the velocity and P_{th} is a uniform pressure related to density and temperature through the equation of state of the fluid:

$$P_{th} = \rho r T \tag{5}$$

where $r = 287\ J.kg^{-1}K^{-1}$ is the ideal gas constant.

Moreover, dynamic viscosity depends on the temperature and follows the Sutherland law, which is valid in the working temperature range of our study [42]:

$$\mu = 1.461 \times 10^{-6} \frac{T^{1.5}}{T + 111} \tag{6}$$

The thermal conductivity is also dependent on the temperature and is derived from the dynamic viscosity and from the constant Prandtl number $Pr = 0.76$:

$$k = \frac{\mu C_p}{Pr} \tag{7}$$

2.2. Numerical model

The flow occurs between two parallel flat plates and Lx and Lz dimensions are periodic (fig. 1). The domain lengths are $2\pi h \times 2h \times (\frac{4}{3})\pi h$ where $h = 0.014923\ m$

The mesh consists of $192 \times 190 \times 128$ cells. It is uniform in the x and z directions. Mesh size follows a hyperbolic tangential law in the y direction in order to be finer close to the walls:

$$y_k = h\left\{1 + \frac{1}{a}\tanh\left[\left(-1 + \frac{k-1}{N-1}\right)\text{artanh}(a)\right]\right\},\ k \in [1, N] \tag{8}$$

Where N is the number of nodes over h (the half-height of the channel) and a is a mesh dilatation parameter. Mesh sizes in wall units are provided in table 1 in the "Main" domain column. The averaging time (normalized by $h/U_{\tau m}$, where $U_{\tau m}$ is the mean friction velocity $U_{\tau m} = (U_{\tau hot} + U_{\tau cold})/2$), is $T^+ \approx 322$. These mesh sharpness and integration time are well positioned with regard to simulations that have shown a good convergence [4], [19]. After $T^+ \approx 200$, heat fluxes at the walls had stabilized and stayed within a range of $\pm 0.1\%$ of their mean values. Moreover a mesh independence check has been performed with a finer mesh ($384 \times 266 \times 384$) when temperature are imposed at the walls, whose mesh sizes in wall units are given in table 1 in the "Check" domain column. The resulting friction values and wall heat fluxes are respectively less than 0.6% and 0.4% different from the main mesh case. The comparison of velocity and temperature means and root-mean-square of velocity fluctuations between the main domain and the check domain exhibits very similar results (fig. 2). The check domain is also larger than the main one (twice as long in the flow direction and 1.5 times larger transversely) and the proximity of the resulting flows (fig. 2) indicates that the study domain is large enough so that no large scale structures are affecting the results. This confirms the observations of a previous study [19] also carried out with a $4\pi h \times 2h \times 2\pi h$ domain size, in which the two-point streamwise and spanwise velocity and temperature correlations fall near zero when the midpoints of the longitudinal and transverse dimensions of the domain are reached respectively.

Table 1: Domain characteristics

	Main	**Check**
Domain size	$2\pi h \times 2h \times \frac{4}{3}\pi h$	$4\pi h \times 2h \times 2\pi h$
Number of cells	$192 \times 190 \times 128$	$384 \times 266 \times 384$
Δx^+	4.64	4.64
Δy^+_{cold}	0.48	0.25
Δy^+_{center}	2.95	2.30
Δy^+_{hot}	0.20	0.10
Δz^+	4.64	2.32
T^+	322	202

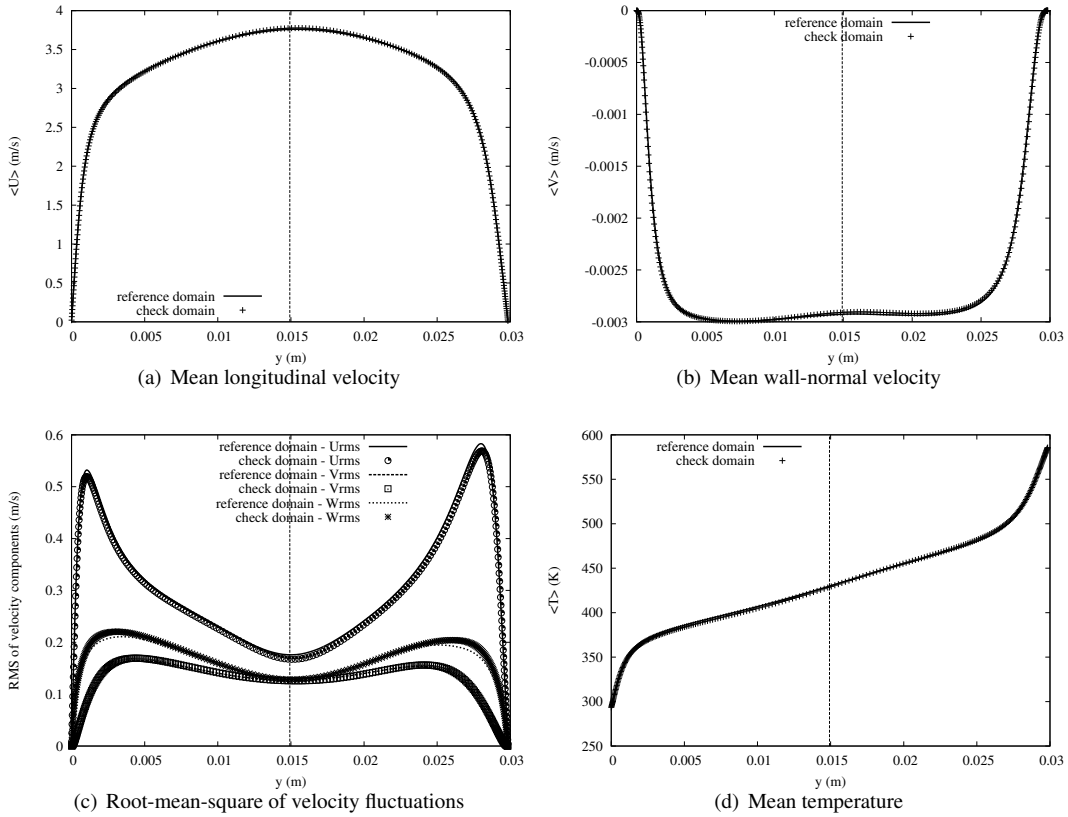

(a) Mean longitudinal velocity

(b) Mean wall-normal velocity

(c) Root-mean-square of velocity fluctuations

(d) Mean temperature

Figure 2: Grid and domain volume independence check

The DNS were carried out with the TrioCFD thermo-hydraulic code [43] created at the French Atomic and Alternative Energies Agency (CEA) and ran on a HPC server provided by the French National Computing Center for Higher Education (CINES). Velocity convection and diffusion are handled by a second order centered scheme. It is the same for temperature diffusion. A third order upstream QUICK scheme (Quadratic Upstream Interpolation for Convective Kinetics) is used for temperature convection. Time integration is handled by a third-order Runge-Kutta numerical scheme.

A couple of comparable simulations with a wall temperature ratio $T_2/T_1 = 2$ is created. First a wall fixed temperature simulation is performed with $T_1 = 293K$ and $T_2 = 586K$, that leads to steady mean heat flux densities at the walls which value is about 1708 W/m^2. These fluxes are then applied as boundary conditions to the wall fixed heat flux simulation.

3. Results and discussion

Statistics are computed by averaging results over the two periodic directions and over time. This averaging is noted by using brackets $< . >$. The mean friction Reynolds number is set to $Re_{\tau m} = 180$, where $Re_{\tau m}$ is the mean value between the turbulent Reynolds numbers taken at the cold and the hot walls:

$$Re_{\tau m} = (Re_{\tau,cold} + Re_{\tau,hot})/2 \tag{9}$$

Each Reynolds number is based on the friction velocity at the corresponding wall:

$$Re_\tau = \frac{U_\tau h}{\nu_w} \tag{10}$$

$$U_\tau = \sqrt{\frac{<\mu_w>}{<\rho_w>}\left.\frac{\partial <U>}{\partial y}\right|_w} \tag{11}$$

Results are normalized using the classical scaling

based on the friction velocity and the friction temperature of the nearest wall:

$$y^+ = \frac{yU_\tau}{\nu_w},\ < U >^+ = \frac{< U >}{U_\tau},\ U^+_{rms} = \frac{U_{rms}}{U_\tau} \qquad (12)$$

$$< T >^+ = \frac{| < T > - < T_w > |}{T_\tau},\ T^+_{rms} = \frac{T_{rms}}{T_\tau} \qquad (13)$$

Table 2: Mean friction variables

Variable	Fixed temperature	Fixed heat flux
$U_{\tau,\ cold}$	0.175	0.173
$U_{\tau,\ hot}$	0.234	0.235
$Re_{\tau,\ cold}$	258	258
$Re_{\tau,\ hot}$	106	106
$T_{\tau,\ cold}$	5.4	5.5
$T_{\tau,\ hot}$	8.1	8.2

Friction variables are presented in table 2. The small differences between fixed temperature and fixed flux simulation friction quantities are not significant enough, when put in balance with the variability due to the grid resolution and the convergence of wall fluxes, to conclude that one of these two simulations is weaker or stronger than the other. In this study, grid and domain size independence have been assessed. Mesh resolutions and simulation times have been set in order to be well positioned when compared to previous studies [19] and the literature [18] [4]. A systematic and detailed estimation of the uncertainties coming from the discretization of the governing equations and the statistical sampling of the data, which is an active and challenging research area [44], has not been performed.

There is a slight relaminarization at the hot wall (suggested by the slight asymmetry of the profile of the mean longitudinal velocity visible in fig. 2(a), the hot side exhibiting more parabolicity than the cold side). Nevertheless, turbulence is not suppressed as the root-mean-squares of all velocity component fluctuations are almost symmetrical with no serious damping at the hot side (fig. 2(c)). The U_{rms} local maximum at the hot-side of the channel is even greater although slightly further from the wall. Relaminarization would be significant for higher temperature gradients [41] and hot to cold wall temperature ratios like $T_2/T_1 = 5$, for which higher friction Reynold number like $Re_{\tau m} = 395$ would be necessary to avoid turbulence suppression as demonstrated in [6].

As shown in fig. 3(a), the mean longitudinal velocity is hardly influenced by the boundary condition type. The difference is even smaller for the root-mean-squares of all velocity components and for the covariance of the longitudinal and the normal velocities presented in fig. 3(c), 3(d), 3(e), and 3(f) respectively. The relative gap is greater for the wall-normal velocity, in particular in the central zone of the channel (fig. 3(b)).

The mean wall-normal velocity is different from zero as can be seen in fig. 2(b) and fig. 3(b), except at the walls where it is forced to zero by the boundary condition. From the equation of energy (Eq. 3), using Eqs. 18 and 5 that formulate the properties of the pressure P_{th}, the following expression can be derived for the divergence of the velocity field:

$$\frac{\partial U_j}{\partial x_j} = \frac{\gamma - 1}{\gamma P_{th}} \frac{\partial}{\partial x_j}(k \frac{\partial T}{\partial x_j}) - \frac{1}{\gamma P_{th}} \frac{dP_{th}}{dt} \qquad (14)$$

In the case of fixed heat flux densities at the walls, averaging and integrating the above eq. 14 leads to the following dependence of the mean wall-normal velocity on the ordinate y [18]:

$$< V >= \frac{\gamma - 1}{\gamma P_{th}} \left(\left\langle k \frac{\partial T}{\partial x_j} \right\rangle - \left\langle k \frac{\partial T}{\partial x_j} \right\rangle \Big|_{\substack{\text{cold} \\ \text{wall}}} \right) \qquad (15)$$

The mean-normal velocity is directly linked with the conservation of energy and with the conductive heat flux crossing each horizontal plane in the channel. It is non-zero except at the walls. The total mean heat flux is constant across the channel and the vertical convective heat flux due to the average wall-normal velocity balances the variation of the mean conductive heat flux. When temperatures are fixed at the walls, eq. 15 is still valid when neglecting the term $\langle P'_{th} \partial_j u'_j \rangle / \langle P_{th} \rangle$. The mean wall-normal velocity is negative and pushes the flow from the hot side towards the cold side of the channel, which is also the denser area [45].

The dimensionless temperature as defined in eq. 13 shows very close profiles, almost independent on the thermal boundary condition type (fig. 4(a)). The same stands for the turbulent wall-normal heat flux (fig. 4(d)). A larger gap can be observed for the turbulent longitudinal heat flux with higher values when the heat flux is fixed (fig. 4(c)), except in the central zone where the gap vanishes. The dimensionless coefficients $U_\tau T_\tau$ of the two kinds of boundary conditions are very close and this gap reflects the real values with a slight attenuation.

The boundary condition type has a major influence on the fluctuations of temperature as shown in fig. 4(b). When the wall temperatures are fixed, the root-mean-square of temperature fluctuations approaches

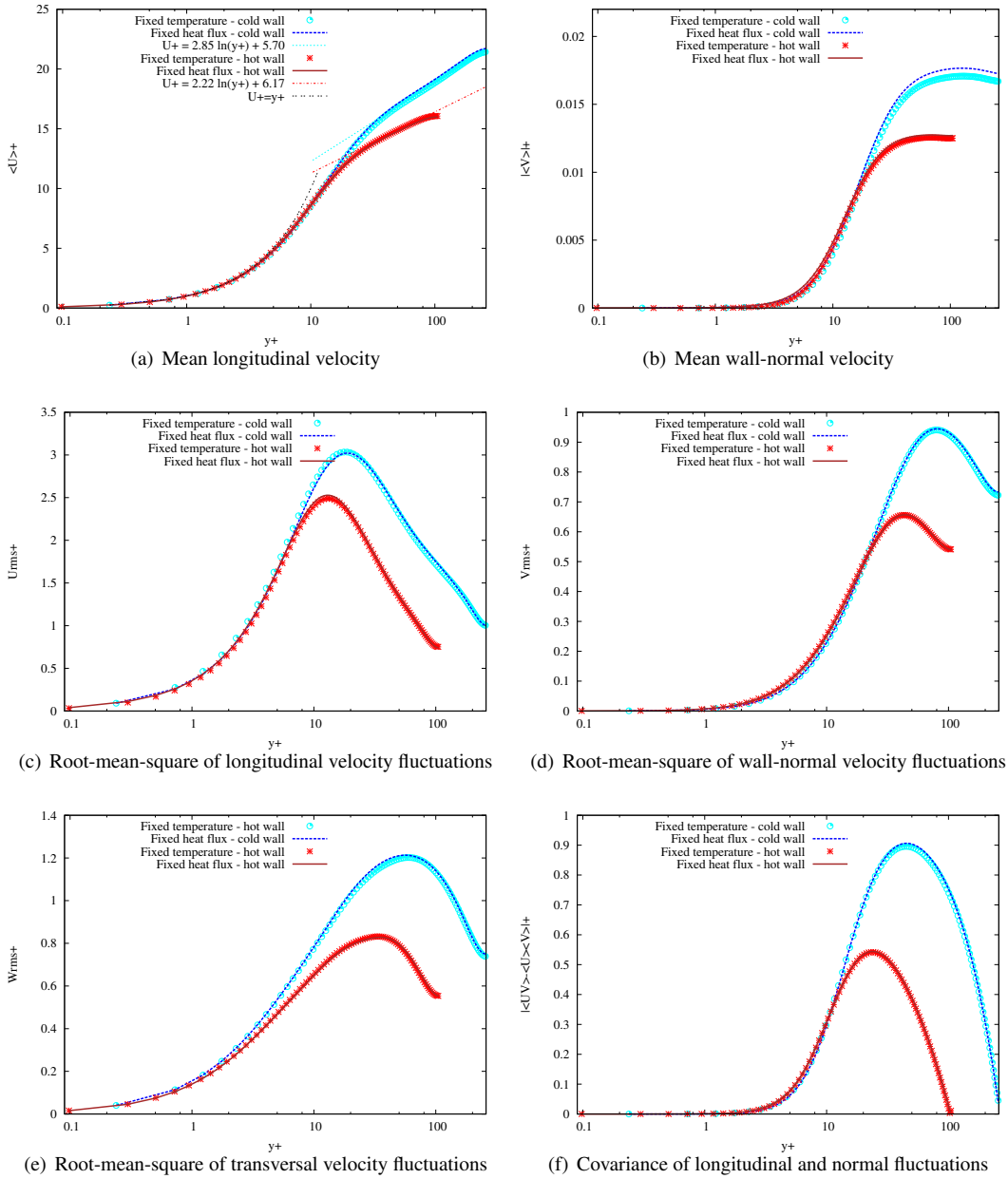

(a) Mean longitudinal velocity

(b) Mean wall-normal velocity

(c) Root-mean-square of longitudinal velocity fluctuations

(d) Root-mean-square of wall-normal velocity fluctuations

(e) Root-mean-square of transversal velocity fluctuations

(f) Covariance of longitudinal and normal fluctuations

Figure 3: Dynamic statistics

zero when getting close to the walls. This is not the case when the heat fluxes are fixed: they are about 2.5 at the hot wall and slightly below 3.0 at the cold wall. These values are compatible with previous studies when taking into account that the wall temperature fluctuations increase when the Reynolds or the Prandtl number increase [23], [30], [31]. The local maximum near the wall is higher and closer to the wall when the heat flux is fixed. The asymmetry of the thermal boundary condition leads to the corresponding asymmetric profiles of the temperature fluctuations. Real T_{rms} are higher at the hot wall than at the cold one. The dimensionless coefficient T_τ is also higher at the hot wall and the net effect leads to a lower dimensionless standard deviation of temperature fluctuations at the hot wall. In the central area of the channel, the temperature fluctuations become

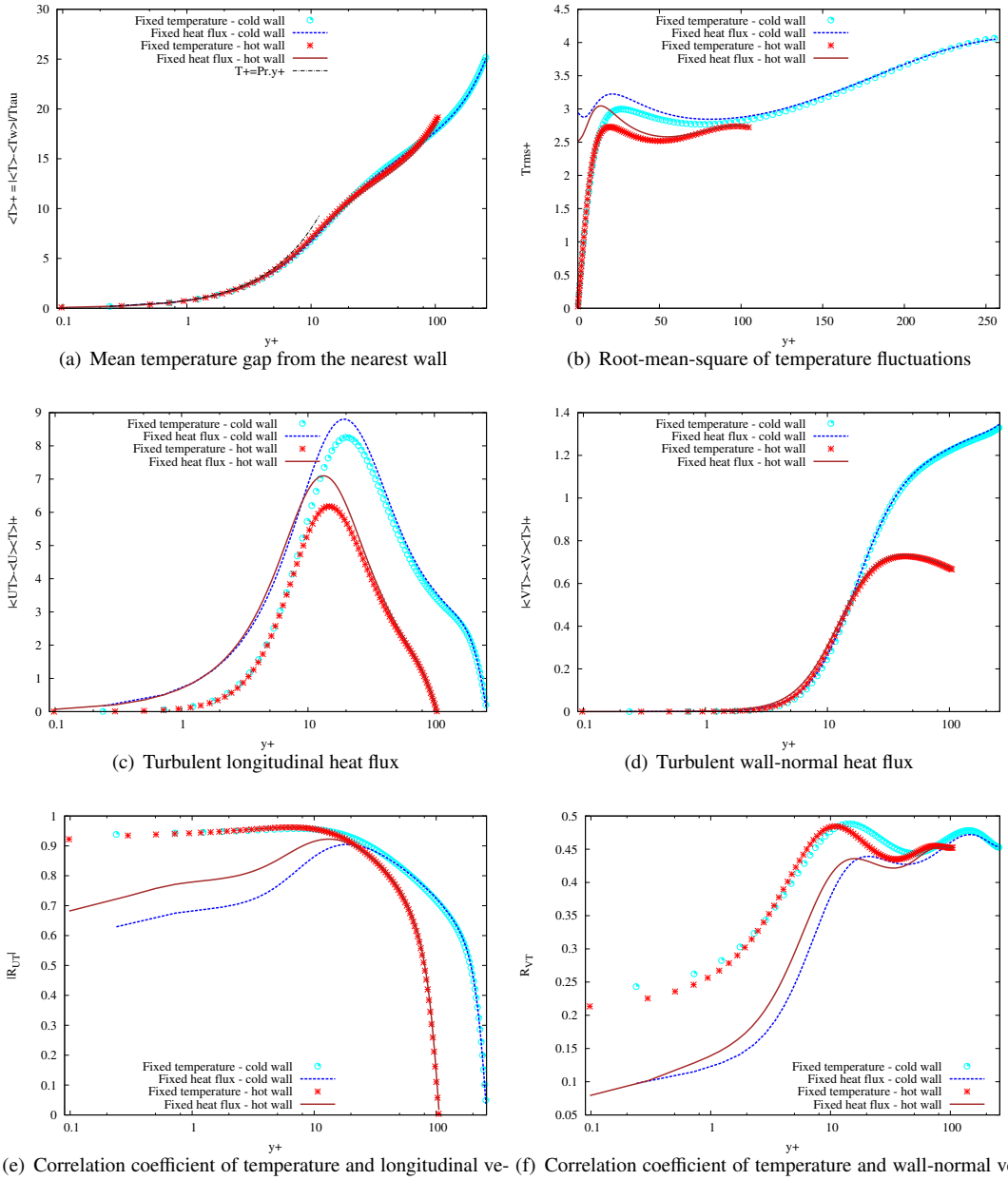

(a) Mean temperature gap from the nearest wall

(b) Root-mean-square of temperature fluctuations

(c) Turbulent longitudinal heat flux

(d) Turbulent wall-normal heat flux

(e) Correlation coefficient of temperature and longitudinal velocity fluctuations

(f) Correlation coefficient of temperature and wall-normal velocity fluctuations

Figure 4: Statistics involving temperature

independent on the boundary condition type. Unlike results from symmetric heating [30] or from a developing flow in an open channel [34], temperature fluctuations do not collapse in the central area: they keep the same order of magnitude across the section.

$$R_{UT} = \frac{< UT > - < U >< T >}{U_{rms} T_{rms}} \qquad (16)$$

$$R_{VT} = \frac{< VT > - < V >< T >}{V_{rms} T_{rms}} \qquad (17)$$

The correlation coefficients R_{UT} (eq. 16) and R_{VT} (eq. 17) combine the behaviors of the turbulent heat fluxes and the standard deviations of temperature and velocities.

In the central area of the channel R_{UT} approaches

zero and is the same whatever the boundary condition type (fig. 4(e)). Indeed, the longitudinal turbulent heat flux vanishes near the centerline while the fluctuations of the temperature and the longitudinal velocity stay finite. Near the walls, the correlation coefficient is higher when wall temperatures are fixed and about 0.9 (in good agreement with value cited by Huang et al. [14]). If the heat flux is imposed, the correlation splits into asymmetric profiles from the hot and the cold wall respectively. The correlation coefficient is higher at the hot wall side of the channel: near the walls (for $y^+ < 10$), the longitudinal turbulent heat flux and the U_{rms} are almost identical whatever the wall side but the T_{rms} are lower at the hot wall and this leads to a greater correlation coefficient.

The correlation coefficient of the temperature and the wall-normal velocity (fig. 4(f)) is lower near the walls when heat fluxes are imposed, because the temperature is free to fluctuate and leads to higher and non-zero T_{rms} while the V_{rms} and the wall-normal heat fluxes are almost independent on the boundary condition type. In the central area of the channel, R_{VT} are closer for the two kinds of boundary conditions as the temperature fluctuations share the same order of magnitude.

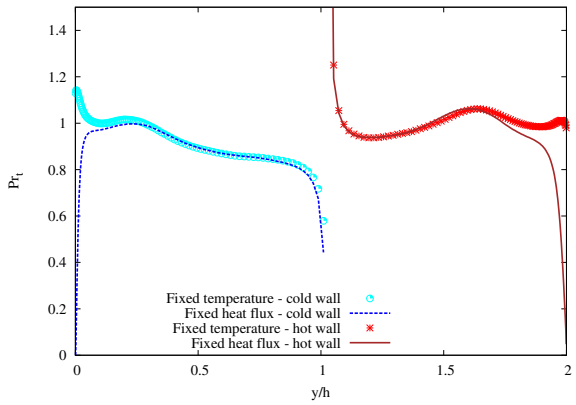

Figure 5: Turbulent Prandtl number Pr_t

$$Pr_t = \frac{(< UV > - < U >< V >)\frac{\partial < T >}{\partial y}}{(< VT > - < V >< T >)\frac{\partial < U >}{\partial y}} \qquad (18)$$

When the temperature is fixed at the walls, the turbulent Prandtl number (eq. 18 and fig. 5) takes values between 0.8 and 1.07 except near the centerline (when $0.95 < y/h < 1.05$) and close to the cold wall (when $y < 0.02$). With fixed wall temperatures, Pr_t is about 1.13 at the cold wall and 0.98 at the hot wall. Near the centerline of the channel, the covariance of the longitudinal and wall-normal velocity fluctuations $< UV > - < U >< V >$ vanishes. It is the same for the normal derivative of the mean longitudinal velocity $\partial < U > /\partial y$. These two zero points do not coincide exactly and their dimensionless distance is around 8×10^{-3}. The Reynolds shear stress zero point happens before the maximum of $< U >$ and this gap leads to a discontinuity and a divergent behavior of the turbulent Prandtl number with a vertical asymptote. This observation is in agreement with a previous study done with a finer grid [19].The discontinuity point is located slightly after the centerline in the hot side of the channel, because of the asymmetry of the boundary conditions. Non-coincidence of the positions of zero shear stress and maximum mean longitudinal velocity have also been observed in other cases where boundary conditions are asymmetric: in turbulent annular concentric pipe flows with asymmetrical curvature effects ([46] [47]) and in fully-developed asymmetric flow in plane channels with different roughening of the planes ([48]).

If heat flux is imposed, the turbulent Prandtl number is hardly changed except near the walls where it vanishes. Both the wall-normal heat flux and the covariance of the longitudinal and normal velocities approach zero when getting close to the walls, but the latter vanishes faster and rules the behavior of the turbulent Prandtl number at the walls.

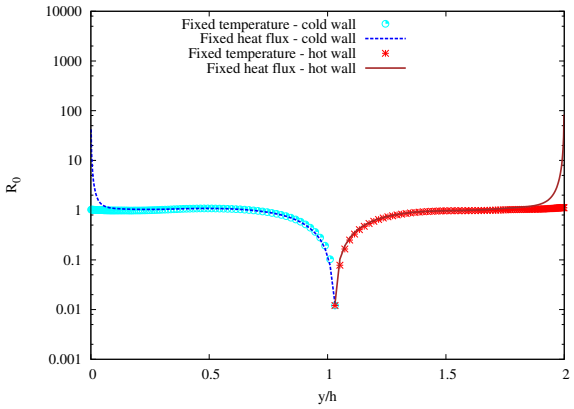

Figure 6: R_0 coefficient (eq. 19) with logarithmic y-scale

$$R_0 = \frac{T_{rms}\left|\frac{\partial < U >}{\partial y}\right|}{U_{rms}\left|\frac{\partial < T >}{\partial y}\right|} \qquad (19)$$

The R_0 coefficient [19] is defined in eq. 19. For fixed temperature walls, R_0 takes values between 0.95 and 1.13 except in the central area (when $0.73 < y/h < 1.44$) where the normal derivative of the mean longitudinal

velocity approaches zero (fig. 6). The assumption $Pr_t \approx \frac{1}{R_0}$ made by Gaviglio [49] is verified with a ±15% relative error with respect to Pr_t except in the centerline vicinity (when $0.67 < y/h < 1.37$) where $\frac{1}{R_0}$ growths or decreases faster than Pr_t. If heat fluxes are imposed at the walls, R_0 diverges when approaching the cold or the hot wall because U_{rms} vanishes while T_{rms} stays finite.

Table 3: Nusselt numbers ($L_c = 2h$)

	Cold wall	**Hot wall**
Present simulations	15	8.5
Dittus − Boelter	31	12
Battista − Perkins	38	15
Jo	28	9

The Nusselt numbers for the hot and cold walls are presented in Table 3, as well as the values obtained using three correlations (Dittus & Boelter [50] in eq. 20, Battista & Perkins [51] in eq. 21 and Jo [52] in eq. 22). All computations are based on the channel height $2h$, on the bulk Reynolds number and on the properties of the fluid at the walls. The temperature of the fluid T_f is taken at the center of the channel.

$$Nu = 0.023 Re^{0.8} Pr^{0.4} \tag{20}$$

$$Nu = 0.021 Re^{0.8} Pr^{0.4} \left(\frac{T_w}{T_f}\right)^{-0.7} \tag{21}$$

$$Nu = 0.0058 Re^{0.9383} Pr^{0.4} \tag{22}$$

The Nusselt number at the hot wall is lower than the one at the cold wall, the thermal conductivity being around 1.6 larger at the hot wall because of its dependency on the temperature. This is also accounted by the three correlations used as a comparison in Table 3. All correlations provide estimates that are significantly larger than the simulation results, the gap being more important at the cold wall. Nevertheless, the aspect ratio of the flat plate bi-periodic channel is very particular and far from the tubular or square geometries at the origin of the correlations. The correlation developed in [52] provides almost exactly the Nusselt value at the hot wall, the gap being still high at the cold wall, although a bit reduced. It is interesting to notice that this last correlation has been developed to fit narrow rectangular channels.

4. Conclusion

In this paper, we have studied the influence of thermal boundary conditions at the walls (fixed temperatures versus imposed heat flux) on a fully developed turbulent channel flow at friction Reynolds number 180 and with a wall temperature ratio of 2. The fluid is an ideal gas and its viscosity and thermal conductivity depend on the temperature. Results show that the longitudinal velocity and the velocity fluctuations are little modified. It is the same for the covariance of the longitudinal velocity and the wall-normal velocity and for the turbulent wall-normal heat flux. Mean temperature also stays almost unchanged. Whatever the boundary condition type, positions of zero shear stress and maximum mean longitudinal velocity are non-coincident and slightly shifted to the hot side of the channel. This leads to a divergent behavior of the turbulent Prandtl number in the central area of the channel.

Other statistics are more impacted by the thermal boundary condition type. This impact appears mainly near the walls, the central area of the channel being almost independent on the boundary condition. The turbulent longitudinal heat flux is higher when the wall heat flux is fixed. The opposite stands for the related correlation coefficient. The correlation coefficient of the temperature and the wall-normal velocity is lower when the heat flux is imposed. The turbulent Prandtl number is also lower and vanishes at the walls when heat fluxes are fixed. The temperature fluctuations are strongly impacted. They keep the same order of magnitude all across the channel and do not vanish at the walls when heat fluxes are fixed. Dimensionless temperature variance is asymmetric and reaches about 2.5 at the hot wall and 3.0 at the cold wall.

5. Acknowledgement

This work was supported by French Investments for the future ("Investissements d'Avenir") programme managed by the National Agency for Research (ANR) under contract ANR-10-LABX-22-01 (labex SOLSTICE). This work was performed using HPC resources from GENCI-CINES (Grants A0022A05099 and A0042A05099). The authors thank the French CEA for providing the CFD software (TrioCFD).

6. References

[1] S. A. Orzag, Analytical theories of turbulence, Journal of Fluid Mechanics 41(02) (1970) 363–386. doi:10.1017/S0022112070000642.

[2] J. Kim, P. Moin, R. Moser, Turbulence statistics in fully developed channel flow at low reynolds number, Journal of Fluid Mechanics 177 (1987) 133–166. doi:10.1017/S0022112087000892.

[3] R. D. Moser, J. Kim, N. N. Mansour, Direct numerical simulation of turbulent channel flow up to $Re_\tau = 590$, Physics of Fluids 11(4) (1999) 943–945. doi:10.1063/1.869966.

[4] A. W. Vreman, J. G. M. Kuerten, Comparison of direct numerical simulation databases of turbulent channel flow at $Re_\tau = 180$, Physics of Fluids 26 (2014) 015102. doi:10.1063/1.4861064.

[5] Y. Morinishi, S. Tamano, E. Nakamura, New scaling of turbulence statistics for incompressible thermal channel flow with different total heat flux gradients, International Journal of Heat and Mass Transfer 50 (9-10) (2007) 1781–1789. doi:10.1016/j.ijheatmasstransfer.2006.10.012.

[6] S. Serra, A. Toutant, F. Bataille, Y. Zhou, Turbulent kinetic energy spectrum in very anisothermal flows, Physics Letters A 376(45) (2012) 3177–3184. doi:10.1016/j.physleta.2012.08.005.

[7] F. Aulery, A. Toutant, F. Bataille, Y. Zhou, Energy transfer process of anisothermal wall-bounded flows, Physics Letters A 379(24-25) (2015) 1520–1526. doi:10.1016/j.physleta.2015.03.022.

[8] F. Aulery, D. Dupuy, A. Toutant, F. Bataille, Y. Zhou, Spectral analysis of turbulence in anisothermal channel flows, Computers & Fluids 151 (2017) 115–131. doi:10.1016/j.compfluid.2016.06.011.

[9] D. Dupuy, A. Toutant, F. Bataille, Turbulence kinetic energy exchanges in flows with highly variable fluid properties, Journal of Fluid Mechanics 834 (2018) 5–54. doi:10.1017/jfm.2017.729.

[10] D. Dupuy, A. Toutant, F. Bataille, Equations of energy exchanges in variable density turbulent flows, Physics Letters A 382(5) (2018) 327–333. doi:10.1016/j.physleta.2017.11.026.

[11] X. Daguenet-Frick, J. M. Foucaut, S. Couderc, A. Toutant, G. Olalde, Experimental analysis of the turbulent flow behavior of a textured surface proposed for asymmetric heat exchangers, Flow Turbulence and Combustion 89 (2012) 149–169. doi:10.1007/s10494-012-9387-y.

[12] E. F. Spina, A. J. Smits, R. S. K., The physics of supersonic turbulent boundary layers, Annu. Rev. Fluid Mech. 26 (1994) 287–319. doi:10.1146/annurev.fluid.26.1.287.

[13] G. Coleman, J. M. Kim, R. D. Moser, A numerical study of turbulent supersonic isothermal-wall channel flow, Journal of Fluid Mechanics 305 (1995) 159–183. doi:10.1017/S0022112095004587.

[14] P. G. Huang, G. N. Coleman, P. Bradshaw, Compressible turbulent channel flows: DNS results and modeling, Journal of Fluid Mechanics 305 (1995) 185–218. doi:10.1017/S0022112095004599.

[15] Y. Morinishi, S. Tamano, K. Nakabayashi, Direct numerical simulation of compressible turbulent channel flow between adiabatic and isothermal walls, Journal of Fluid Mechanics 502 (2004) 273–308. doi:10.1017/S0022112003007705.

[16] S. Tamano, Y. Morinishi, Effect of different wall boundary conditions on compressible turbulent channel flow at $M = 1.5$, Journal of Fluid Mechanics 548 (2006) 361–373. doi:10.1017/S0022112005007639.

[17] M. S. Shadloo, A. Hadjadj, H. F., Statistical behavior of supersonic turbulent boundary layers with heat transfer at $M_\infty = 2$, International Journal of Heat and Fluid Flow 53 (2015) 113–134. doi:10.1016/j.ijheatfluidflow.2015.02.004.

[18] F. Nicoud, Conservative high-order finite-difference schemes for low Mach number flows, Journal of Computational Physics 158 (2000) 71–97. doi:10.1006/jcph.1999.6408.

[19] A. Toutant, F. Bataille, Turbulence statistics in a fully developed channel flow submitted to a high temperature gradient, International Journal of Thermal Sciences 74 (2013) 104–118. doi:10.1016/j.ijthermalsci.2013.06.003.

[20] S. Dharmarathne, M. Tutkun, G. Araya, L. Castillo, Structures of scalar transport in a turbulent channel, European Journal of Mechanics B/Fluids 55 (2016) 259–271. doi:10.1016/j.euromechflu.2015.06.010.

[21] M. Ould-Rouiss, M. Bousbai, A. Mazouz, Large eddy simulation of turbulent heat transfer in pipe flows with respect to reynolds and prandtl number effects, Acta Mech. 224 (2013) 1133–1155. doi:10.1007/s00707-012-0796-8.

[22] L. Redjem-Saad, M. Ould-Rouiss, G. Lauriat, Direct numerical simulation of turbulent heat transfer in pipe flows: Effect of prandtl number, International Journal of Heat and Fluid Flow 28 (2007) 847–861. doi:10.1016/j.ijheatfluidflow.2007.02.003.

[23] M. Ould-Rouiss, L. Redjem-Saad, G. Lauriat, A. Mazouz, Effect of prandtl number on the turbulent thermal field in annular pipe flow, International Communications in Heat and Mass Transfer 37 (2010) 958–963. doi:10.1016/j.icheatmasstransfer.2010.06.027.

[24] M. Ould-Rouiss, L. Redjem-Saad, G. Lauriat, Direct numerical simulation of turbulent heat transfer in annuli: Effect of heat flux ratio, International Journal of Heat and Fluid Flow 30 (2009) 579–589. doi:10.1016/j.ijheatfluidflow.2009.02.018.

[25] M. Ould-Rouiss, A. Dries, A. Mazouz, Numerical predictions of turbulent heat transfer for air flow in rotating pipe, International Journal of Heat and Fluid Flow 31 (2010) 507–517. doi:10.1016/j.ijheatfluidflow.2010.02.015.

[26] M. Bousbai, M. Ould-Rouiss, A. Mazouz, A. Mataoui, Turbulent heat transfer characteristics of water flow in a rotating pipe, Heat Mass Transfer 49 (2013) 469–484. doi:10.1007/s00231-012-1094-7.

[27] N. Kasagi, A. Kuroda, Y. Tomita, Direct numerical simulations of passive scalar field in a turbulent channel flow, Transaction of the ASME 114 (1992) 598–606. doi:10.1115/1.2911323.

[28] H. Kawamura, K. Ohsaka, H. Abe, K. Yamamoto, DNS of turbulent heat transfer in channel flow with low to medium-high prandtl number fluid, International Journal of Heat and Fluid Flow 19 (1998) 482–491. doi:10.1016/S0142-727X(98)10026-7.

[29] R. Bergant, I. Tiselj, Near-wall passive scalar transport at high prandtl numbers, Physics of Fluids 19 (2007) 065105. doi:10.1063/1.2739402.

[30] C. Flageul, S. Benhamadouche, E. Lamballais, D. Laurence, DNS of turbulent channel flow with conjugate heat transfer: Effect of thermal boundary conditions on the second moments and budgets, International Journal of Heat and Fluid Flow 55 (2015) 34–44. doi:10.1016/j.ijheatfluidflow.2015.07.009.

[31] I. Tiselj, Tracking of large-scale structures in turbulent channel with direct numerical simulation of low prandtl number passive scalar, Physics of Fluids 26 (2014) 125111. doi:10.1063/1.4905018.

[32] I. Tiselj, C. L., DNS of turbulent channel flow with conjugate heat transfer at prandtl number 0.01, Nuclear Engineering and Design 253 (2012) 153–160. doi:10.1016/j.nucengdes.2012.08.008.

[33] I. Tiselj, R. Bergant, B. Mavko, I. Bajsic, G. Hetsroni, DNS of turbulent heat transfer in channel flow with heat conduction in the solid wall, Journal of Heat Transfer 123 (2001) 849–847. doi:10.1115/1.1389060.

[34] M. Bellec, A. Toutant, G. Olalde, Large eddy simulations of thermal boundary layer developments in a turbulent channel flow under asymmetrical heating, Computers and fluids 151 (2017) 159–176. doi:10.1016/j.compfluid.2016.07.001.

[35] G. K. Batchelor, An introduction to fluid dynamics, Cambridge University Press, 2000.

[36] R. L. Panton, Incompressible flow, John Wiley & Sons, 2013.

[37] S. Paolucci, On the filtering of sound from the navier-stokes equations, Tech. Rep. SAND82-8257, Livermore: Scandia National Laboratories.

[38] T. L. Bergman, A. S. Lavine, F. P. Incropera, D. P. Dewitt, Fundamentals of heat and mass transfer, John Wiley & Sons, 2011.

[39] O. Aydin, W.-J. Yang, Mixed convection in cavities with locally heated lower wall and moving sidewalls, Numerical Heat Transfer, Part A: Applications: An International Journal of Computation and Methodolog 37(7) (2000) 695–710. doi:10.1080/104077800274037.

[40] W. Jing, T. Tao, L. Xiyuan, P. Yifei, Analysis on influence of gravity on convection heat transfer in manned spacecraft during terrestrial test, International Journal of Aerospace and Mechanical Engineering 6(9) (2012) 1908–1913.

[41] B. Lessani, M. V. Papalexandris, Time-accurate calculation of variable density flows with strong temperature gradients and combustion, Journal of Computational Physics 212 (2006) 218–246. doi:10.1016/j.jcp.2005.07.001.

[42] W. Sutherland, The viscosity of gases and molecular force, Philosophical Magazine Series 5 36:223 (1893) 507–531. doi:10.1080/14786449308620508.

[43] C. Calvin, O. Cueto, P. Emonot, An object-oriented approach to the design of fluid mechanics software, ESAIM: Mathematical Modeling and Numerical Analysis 36(05) (2002) 907–921. doi:10.1051/m2an:2002038.

[44] T. A. Oliver, M. Malaya, R. Ulerich, R. D. Moser, Estimating uncertainties in statistics computed from direct numerical simulation, Physics of Fluids 26, 035101. doi:10.1063/1.4866813.

[45] I. Eames, J. C. R. Hunt, Inviscid flow around bodies moving in weak density gradients without buoyancy effects, Journal of Fluid Mechanics 353 (1997) 331–355. doi:10.1017/S002211209700760X.

[46] K. Rehme, Turbulent flow in smooth concentric annuli with small radius ratios, Journal of Fluid Mechanics 64(2) (1974) 263–287. doi:10.1017/S0022112074002394.

[47] K. Rehme, Turbulence measurements in smooth concentric annuli with small radius ratios, Journal of Fluid Mechanics 72(1) (1975) 189–206. doi:10.1017/S0022112075003023.

[48] K. Hanjalic, B. E. Launder, Fully developed asymmetric flow in a plane channel, Journal of Fluid Mechanics 51(2) (1972) 301–335. doi:10.1017/S0022112072001211.

[49] J. Gaviglio, Reynolds analogies and experimental study of heat transfer in supersonic boundary layer, International Journal of Heat and Mass Transfer 30(05) (1987) 911–926. doi:10.1016/0017-9310(87)90010-X.

[50] F. W. Dittus, L. M. K. Boelter, Heat transfer in automobile radiators of the tubular type, International Communications in Heat and Mass Transfer 12 (1985) 3–22.

[51] E. Battista, H. C. Perkins, Turbulent heat and momentum transfer in a square duct with moderate property variations, International Journal of Heat and Mass Transfer 13 (1970) 1063–1065. doi:10.1016/0017-9310(70)90172-9.

[52] D. Jo, R. M. Al-yahia, R. M. Altamini, J. Park, H. Chae, Experimental investigation of convective heat transfer in narrow rectangular channel for upward and downward flows, Nuclear Engineering and Technology 46(2) (2014) 195–206. doi:10.5516/NET.02.2013.057.